Flu Di erence Splitting and the Balancing of Source Terms and Flu Gradients. *

M.E.Hubbard

Th Univ rsity of R ading, D partm nt of Math matics,

P.O.Box 220, Whit knights, R ading, B rkshir , RG6 6AX, U.K.

and

P.Garcia-Navarro

Ar a d M canica d Fluidos, C ntro Polit cnico Sup rior,

C/Maria d Luna 3, 50015 Zaragoza, España.

21st May 1999

*This work has been carried out as part of the Oxford/Reading Institute for Computational Fluid Dynamics and was funded by EPSRC.

1 Introduction

There has been much research in CFD into the accurate and efficient solution of homogeneous systems of conservation laws. More recently, as numerical models become more complicated and the areas of application of these methods widens, it has become important that other aspects of the discretisation be given due attention. This is certainly true in the field of computational hydraulics where

regular and irregular grids in any num

which has yet to be approximated. For convenience, a cell centre scheme in which the control volumes coincide with the mesh cells has been considered throughout this work, although the ideas may be applied to other types of sc

an approximate Riemann solver to decompose the flux terms into characteristic components by diagonalisation of the homogeneous part of a linearised form of the system (2.1), which is

$$\underline{U}_t + \tilde{\mathbf{A}}\underline{U}_x \;=\; \underline{0}\,, \tag{2.4}$$

where $\tilde{\mathbf{A}} \approx \frac{\partial \underline{F}}{\partial \underline{U}}$ is the linearised flux Jacobian of the system. The Riemann problems arise at the interfaces between the control volumes (the mesh nodes in this case) where discontinuities occur in the discrete representation of the solution.

Application of Roe's Riemann solver results in a decoupling of the linearised equations that splits the flux difference so that it can be written in a number of equivalent forms, *i.e.* at an interface

$\Delta \underline{F}_i$

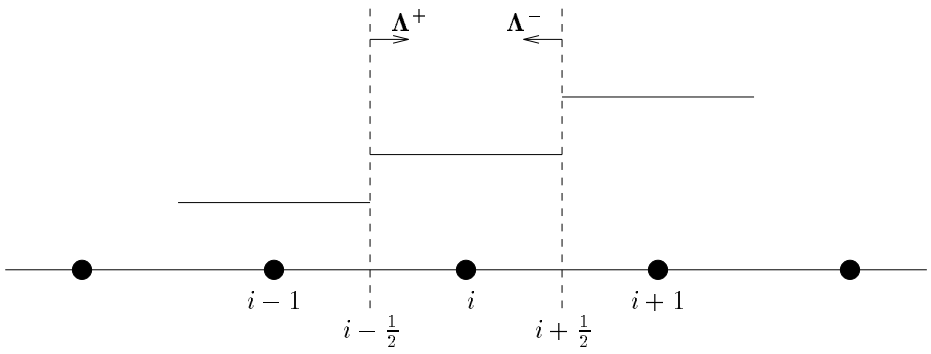

Figure 2.2: Wave propagation directions in a control volume.

Choosing the Roe-average state (represented by $\tilde{\cdot}$) to satisfy (2.5) means that the resulting approximate Riemann solver is an exact solver for this local linearisation of the Riemann problem. More importantly, in the context of this work, when (2.5) is combined with (2.6) the nodal update scheme given by (2.2) is equivalent to the fluctuation-signal scheme [12] given by

$$\underline{U}_i^{n+1} \;=\; \underline{U}_i^n - \frac{\Delta t}{\Delta x_i}\left[\left(\tilde{\mathbf{R}}\tilde{\mathbf{\Lambda}}^-\tilde{\mathbf{R}}^{-1}\Delta\underline{U}\right)_{i+\frac{1}{2}} + \left(\tilde{\mathbf{R}}\tilde{\mathbf{\Lambda}}^+\tilde{\mathbf{R}}^{-1}\Delta\underline{U}\right)_{i-\frac{1}{2}}\right] + \frac{\Delta t}{\Delta x_i}\,\underline{\mathbf{S}}_i^*\,, \quad (2.7)$$

in which

$$\tilde{\mathbf{\Lambda}}^\pm \;=\; \frac{1}{2}(\tilde{\mathbf{\Lambda}} \pm |\tilde{\mathbf{\Lambda}}|)\,. \quad (2.8)$$

This splits the update into contributions related to right-going (+) and left-going (−) characteristics in the decomposition. It follows that the solution is updated using only contributions from the wave perturbations of the Riemann problems at the nodes which enter the cell under consideration, as illustrated in Figure 2.2. It remains to choose an appropriate form for the numerical source term integral $\underline{\mathbf{S}}^*$.

2.1 Source terms

This work follows much recent research into source term discretisation, see for example [5, 6, 1, 4], which has concentrated on the use of a characteristic decomposition of the type shown in (2.5). This similarly projects the source term integral onto the eigenvectors of the flux Jacobian $\tilde{\mathbf{A}}$, so that in its linearised

form it can be expressed as

$$\int_{x_i}^{x_{i+1}} \underline{S}\,\mathrm{d}x \;\approx\; \underline{\tilde{\mathbf{S}}}_{i+\frac{1}{2}} \;=\; \left(\tilde{\mathbf{R}}\,\tilde{\mathbf{R}}^{-1}\underline{\tilde{\mathbf{S}}}\right)_{i+\frac{1}{2}} \;=\; \left(\sum_{k=1}^{N_w} \tilde{\beta}_k \underline{\tilde{r}}_k\right)_{i+\frac{1}{2}}, \tag{2.9}$$

where $\tilde{\beta}_k$, the coefficients of the decomposition, are the components of the vector $\tilde{\mathbf{R}}^{-1}\underline{\tilde{\mathbf{S}}}$. Note that the integral approximated in (2.9) is over a dual cell of the mesh (associated with the interface $i+\frac{1}{2}$), and can be easily incorporated within the fluctuation-signal form of the finite volume scheme given by (2.7). $\underline{\mathbf{S}}_i^*$ will be constructed out of contributions from both ends of the cell, with consistency assured as long as the whole of each dual cell integral (2.9) is distributed.

It is useful (though less so than in higher dimensions) to note here that the analytical form of the source term can be split up into components which can be discretised separately, *i.e.*

$$\underline{S} \;=\; \underline{S}^0 + \sum_j \underline{S}_j^1 \frac{\partial S_j^2}{\partial x}, \tag{2.10}$$

so that its integral can be approximated consistently by

$$\int_{x_i}^{x_{i+1}} \underline{S}\,\mathrm{d}x \;\approx\; \underline{\tilde{\mathbf{S}}}_{i+\frac{1}{2}} \;=\; \left(\Delta x \underline{\tilde{S}}^0 + \sum_j \underline{\tilde{S}}_j^1\, \Delta S_j^2\right)_{i+\frac{1}{2}}, \tag{2.11}$$

and comparison with (2.9) leads directly to the coefficients $\tilde{\beta}_k$ of the characteristic decomposition of $\underline{\tilde{\mathbf{S}}}_{i+\frac{1}{2}}$.

The terms within the sum on the right hand side of (2.11) may be called upon to balance components of the flux difference $\Delta\underline{F}$ (2.5) so they must be linearised in the same way to ensure that, for the chosen equilibrium state,

$$\underline{F}_x - \underline{S} \;\equiv\; \underline{0} \quad\Rightarrow\quad \Delta\underline{F}_{i+\frac{1}{2}} - \underline{\tilde{\mathbf{S}}}_{i+\frac{1}{2}} \;=\; \underline{0} \tag{2.12}$$

throughout the domain. This follows because at this equilibrium the decompositions (2.5) and (2.9) have been constructed to give $\tilde{\mathbf{\Lambda}}\tilde{\mathbf{R}}^{-1}\,\Delta\underline{U} = \tilde{\mathbf{R}}^{-1}\underline{\tilde{\mathbf{S}}}$ (or alternatively $\tilde{\alpha}_k\tilde{\lambda}_k = \tilde{\beta}_k$). Hence $\tilde{\cdot}$ still represents the evaluation of a quantity at the Roe-average state.

The first term on the right hand side of (2.11) contains only contributions which provide no exact balance with the flux derivatives (*e.g.* bed friction terms in the shallow water equations), so the precise form of their linearisation is not

prescribed by the above arguments. However, it seems sensible that they should also be evaluated at the same state, given by the Roe-average.

As a result of the characteristic decomposition (2.9), the source terms may be discretised in an 'upwind' manner (although, since none of the components has an inherent upwind direction, this must be taken from the corresponding flux component). This leads straightforwardly to an appropriate upwind fluctuation-signal formulation for the first order scheme (2.7) with source terms, given by

$$\begin{aligned} \underline{U}_i^{n+1} &= \underline{U}_i^n - \frac{\Delta t}{\Delta x_i}\left[\left(\tilde{\mathbf{R}}(\tilde{\mathbf{\Lambda}}^-\tilde{\mathbf{R}}^{-1}\Delta\underline{U} - \mathbf{I}^-\tilde{\mathbf{R}}^{-1}\underline{\tilde{\mathbf{S}}})\right)_{i+\frac{1}{2}}\right. \\ &\qquad \left. + \left(\tilde{\mathbf{R}}(\tilde{\mathbf{\Lambda}}^+\tilde{\mathbf{R}}^{-1}\Delta\underline{U} - \mathbf{I}^+\tilde{\mathbf{R}}^{-1}\underline{\tilde{\mathbf{S}}})\right)_{i-\frac{1}{2}}\right], \end{aligned} \tag{2.13}$$

in which $\mathbf{I}^\pm = \tilde{\mathbf{\Lambda}}^{-1}\tilde{\mathbf{\Lambda}}^\pm$. The correct balance follows immediately from (2.12).

It is not immediately clear though, how the discretisation of the source term implied by (2.13) can be converted into a numerical source integral $\underline{\mathbf{S}}_i^*$ so that the same balance can be achieved within the flux-based for^^TD4sothat..sedTJ4vmannwbdiscretpa

$$- \left(\tilde{\mathbf{R}}(|\tilde{\mathbf{\Lambda}}|\tilde{\mathbf{R}}^{-1}\Delta\underline{U} - \mathrm{sgn}(\mathbf{I})\tilde{\mathbf{R}}^{-1}\underline{\tilde{\mathbf{S}}}) \right)_{i-\frac{1}{2}} \Bigg] \,, \qquad (2.14)$$

in which $\mathrm{sgn}(\mathbf{I}) = \tilde{\mathbf{\Lambda}}^{-1}|\tilde{\mathbf{\Lambda}}|$. Since (2.5) and (2.9) hold, and

$$\Delta\underline{F}_{i+\frac{1}{2}} + \Delta\underline{F}_{i-\frac{1}{2}} \;=\; (\underline{F}_{i+1} + \underline{F}_i) - (\underline{F}_i + \underline{F}_{i-1}) \,, \qquad (2.15)$$

it follows that the scheme (2.14) can be simplified to

$\underline{U}$

and $\underline{\mathbf{S}}^*$ becomes obsolete. In some cases it may also be possible to incorporate some part of the source term which can be expressed as a derivative within the numerical flux, and then apply an appropriate discretisation to the remaining component of the source.

2.1.1 Flux limited schemes

The approach presented in the previous section is no different to the standard upwind technique for approximating source terms when a first order upwind flux discretisation is being used [5]. The only new aspect is the way it has been written, splitting the dual cell source integral into two parts. Usually though, accuracy of higher than first order is required for practical calculations.

The accuracy of Roe's scheme is improved, without introducing spurious oscillations into the solution, by the application of flux limiting techniques [15, 8]. These ensure second order accuracy in smooth regions of the flow, whilst enforcing a Total Variation Diminishing (TVD) property. It is achieved by including a high order correction term in the numerical flux, which becomes [13]

$$\underline{F}^*_{i+\frac{1}{2}} = \frac{1}{2}\left(\underline{F}_{i+1} + \underline{F}_i\right) - \frac{1}{2}\left(\tilde{\mathbf{R}}|\tilde{\mathbf{\Lambda}}|\mathbf{L}\tilde{\mathbf{R}}^{-1}\Delta\underline{U}\right)_{i+\frac{1}{2}} , \tag{2.21}$$

in which $\mathbf{L} = \mathrm{diag}(1 - L(r_{ki}$

with a similar expression for $\underline{\mathbf{S}}^*_{i-\frac{1}{2}}{}^+$ in (2.17). Note that since (2.23) is an edge-based quantity, it is simple to evaluate with the fluxes and include within the numerical model.

At this point it should be emphasised that the TVD condition which the flux limiter has been constructed to satisfy applies to the homogeneous system of conservation laws, and the inclusion of source terms means that spurious oscillations may appear in the final solution. The same is true of the slope limited schemes of the next section. This problem has not been addressed in this work.

2.1.2 Slope limited schemes

The same balance is slightly more difficult to achieve when the high resolution scheme is constructed using a MUSCL-type slope limiting approach [17]. This is because the underlying representation of the solution is now taken to be linear within each cell so that (2.15) is no longer true. It can though, be replaced by the more general expression,

$$\Delta\underline{F}_{i+\frac{1}{2}} + \Delta\underline{F}_{i-\frac{1}{2}} \;=\; (\underline{F}^{\mathrm{R}}_{i+\frac{1}{2}} + \underline{F}^{\mathrm{L}}_{i+\frac{1}{2}}) - (\underline{F}^{\mathrm{R}}_{i-\frac{1}{2}} + \underline{F}^{\mathrm{L}}_{i-\frac{1}{2}}) - 2(\underline{F}^{\mathrm{L}}_{i+\frac{1}{2}} - \underline{F}^{\mathrm{R}}_{i-\frac{1}{2}})\,, \quad (2.24)$$

where the superscripts $\cdot^{\mathrm{R}}$ and $\cdot^{\mathrm{L}}$ represent evaluation on, respectively, the right and left hand sides of the interface indicated by the associated subscript (as shown in Figure 2.4). The corresponding numerical flux is

$$\underline{F}^*_{i+\frac{1}{2}} \;=\; \frac{1}{2}\left(\underline{F}^{\mathrm{R}}_{i+\frac{1}{2}} + \underline{F}^{\mathrm{L}}_{i+\frac{1}{2}}\right) - \frac{1}{2}\left(\tilde{\mathbf{R}}|\tilde{\mathbf{\Lambda}}|\tilde{\mathbf{R}}^{-1}\Delta\underline{U}\right)_{i+\frac{1}{2}}\,, \quad (2.25)$$

in which the Roe-averages are now evaluated from the reconstructed piecewise linear solution. An appropriate correction must therefore be made to the numerical source within each cell, and this leads to

$$\underline{\mathbf{S}}^*_i \;=\; \left(\underline{\mathbf{S}}^*_{i+\frac{1}{2}}{}^- + \underline{\mathbf{S}}^*_{i-\frac{1}{2}}{}^+\right) - \tilde{\underline{\mathbf{S}}}\left(\underline{U}^{\mathrm{L}}_{i+\frac{1}{2}}, \underline{U}^{\mathrm{R}}_{i-\frac{1}{2}}\right)\,. \quad (2.26)$$

The first term on the right hand side is evaluated precisely as before, in (2.17), except that the interface values are now those of the MUSCL reconstruction of the solution within each cell. $\tilde{\underline{\mathbf{S}}}$ is simply the source term integral approximated over the mesh cell (*cf.* (2.11)), and hence evaluated at the Roe-average of the left and right states of the linear reconstruction of the solution within the cell. In

terms of the approximations (2.12) and (2.11) the extra term can be thought of as a correction to the integral of the source term over the dual cell arising from the linear variation of the approximation.

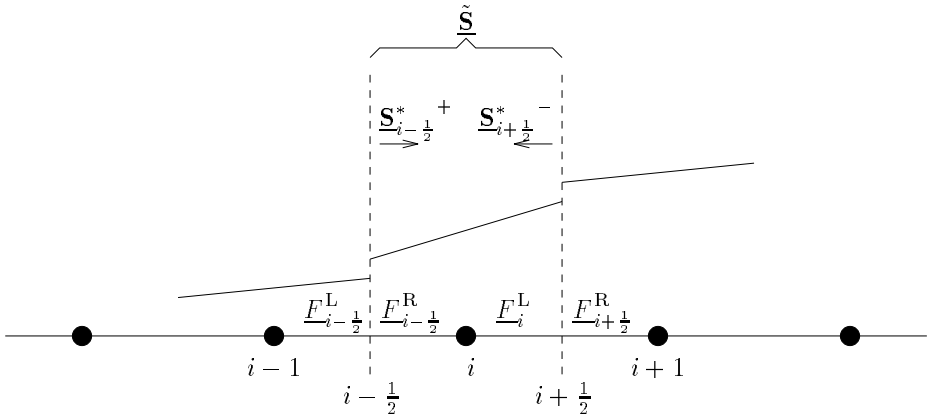

appropriate state of equilibrium (*cf.* (2.11) in which the equilibrium was achieved automatically using the original averages).

Following the same steps as in Section 2 to transform the fluctuation-signal scheme to the flux-based scheme, but including this extra term in the flux difference, leads to precisely the same form for the scheme when approximating the homogeneous system as shown in (2.2), but with new expressions for the numerical fluxes, given by

$$\underline{F}^*_{i+\frac{1}{2}} \;=\; \frac{1}{2}\,(\underline{F}_{i+1} + \underline{F}_i) - \frac{1}{2}\left(\tilde{\mathbf{R}}|\tilde{\mathbf{\Lambda}}|\tilde{\mathbf{R}}^{-1}\,\Delta\underline{U} + \tilde{\mathbf{R}}\,\mathrm{sgn}(\mathbf{I})\tilde{\mathbf{R}}^{-1}\underline{\tilde{V}}\right)_{i+\frac{1}{2}}\,, \qquad (2.28)$$

in the first order case,

$$\underline{F}^*_{i+\frac{1}{2}} \;=\; \frac{1}{2}\,(\underline{F}_{i+1} + \underline{F}_i)$$

In these equations d is the depth of the flow, h is the depth of the bed below a nominal still water level, $b = b(x)$ is the channel breadth, u is the flow velocity, and g is the acceleration due to gravity. These quantities are depicted in Figure 2.5.

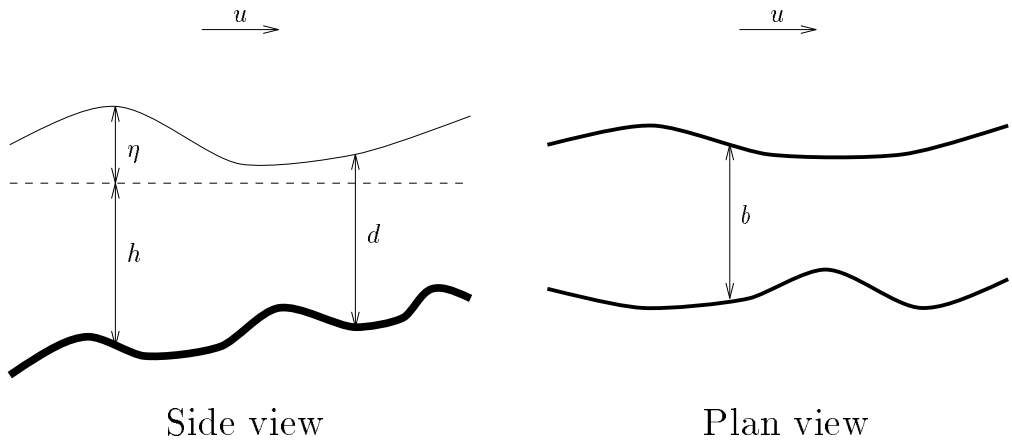

Figure 2.5: The shallow water flow variables.

Equation (2.31) provides an example which includes source terms and a spatial dependence on channel breadth which is independent of the flow. Furthermore, the balance which has been sought in previous sections is illustrated by the steady state represented by still water ($d \equiv h$ and $u \equiv 0$), in which case the system (2.31) reduces to

$$\left(\frac{1}{2}gbd^2\right)_x = \frac{1}{2}gd^2b_x + gbdh_x\,. \tag{2.33}$$

Previously it has only been possible to maintain this steady state numerically when first order schemes have been used.

The characteristic decomposition (2.27) for the one-dimensional shallow water equations (2.31) and (2.32) is completely defined by

$$\begin{aligned}
\tilde{\alpha}_1 &= \frac{\Delta(bd)}{2} + \frac{1}{2\tilde{c}}\left(\Delta(bdu) - \tilde{u}\,\Delta(bd)\right)\,, \quad \tilde{\alpha}_2 = \frac{\Delta(bd)}{2} - \frac{1}{2\tilde{c}}\left(\Delta(bdu) - \tilde{u}\,\Delta(bd)\right) \\
\tilde{\lambda}_1 &= \tilde{u} + \tilde{c}\,, \quad \tilde{\lambda}_2 = \tilde{u} - \tilde{c} \\
\underline{\tilde{r}}_1 &= \begin{pmatrix} 1 \\ \tilde{u} + \tilde{c} \end{pmatrix}\,, \quad \underline{\tilde{r}}_2 = \begin{pmatrix} 1 \\ \tilde{u} - \tilde{c} \end{pmatrix} \\
\tilde{\gamma}_1 &= -\frac{1}{4g}\tilde{c}^3\Delta b\,, \quad \tilde{\gamma}_2 = \frac{1}{4g}\tilde{c}^3\Delta b\,,
\end{aligned} \tag{2.34}$$

and it is easily shown that (2.27) is satisfied exactly when

$$\tilde{u} \;=\; \frac{\sqrt{b^{\mathrm{R}}d^{\mathrm{R}}}u^{\mathrm{R}} + \sqrt{b^{\mathrm{L}}d^{\mathrm{L}}}u^{\mathrm{L}}}{\sqrt{b^{\mathrm{R}}d^{\mathrm{R}}} + \sqrt{b^{\mathrm{L}}d^{\mathrm{L}}}}\,, \quad \tilde{c}^2 \;=\; g\left(\frac{\sqrt{b^{\mathrm{R}}}d^{\mathrm{R}} + \sqrt{b^{\mathrm{L}}}d^{\mathrm{L}}}{\sqrt{b^{\mathrm{R}}} + \sqrt{b^{\mathrm{L}}}}\right)\,, \tag{2.35}$$

which reduce to the Roe-averages for one-dimensional shallow water flow described in [5] in the absence of breadth variation (*i.e.* when $b^{\mathrm{R}} = b^{\mathrm{L}}$). The corresponding decomposition of the source terms (2.9) then leads to

$$\tilde{\beta}_1 \;=\; \frac{1}{4g}\tilde{c}^3\Delta b + \frac{1}{2}\tilde{b}\tilde{c}\Delta h \;=\; -\tilde{\beta}_2 \tag{2.36}$$

In order for (2.18) and (2.19) to maintain the correct balance, *i.e.*

$$\tilde{\alpha}_k\tilde{\lambda}_k + \tilde{\gamma}_k - \tilde{\beta}_k \;=\; 0 \qquad \forall k \tag{2.37}$$

or equivalently,

$$\tilde{\mathbf{R}}\left(\tilde{\mathbf{\Lambda}}\tilde{\mathbf{R}}^{-1}\,\Delta\underline{U} + \tilde{\mathbf{R}}^{-1}\underline{\tilde{V}} - \tilde{\mathbf{R}}^{-1}\underline{\tilde{\mathbf{S}}}\right) \;=\; \underline{0} \tag{2.38}$$

when the flow is quiescent, $\tilde{b}$ is constructed so that it satisfies

$$\tilde{b}\Delta h \;=\; \Delta(bh) - \tilde{h}\Delta b\,, \tag{2.39}$$

where $\tilde{h}$ is ev

These have been studied using a variety of channel geometries.

The geometry for the first test case was proposed by the Working Group On Dam-Break Modelling [3], and the bed and breadth variation of the channel (of length 1500) are depicted in Figure 2.6. The upwind source term treatment described in this paper is compared with a much simpler pointwise discretisations in Figure 2.7 (using a uniform 600 cell grid, so that $\Delta x = 2.5$), which show graphs of water surface level and unit discharge for the numerical steady states which result from quiescent initial conditions ($\eta = d - h = 12.0$ and $u = 0.0$), and applying simple non-reflecting boundary conditions. In this case the initial (still water) conditions should be maintained indefinitely by the numerical scheme.

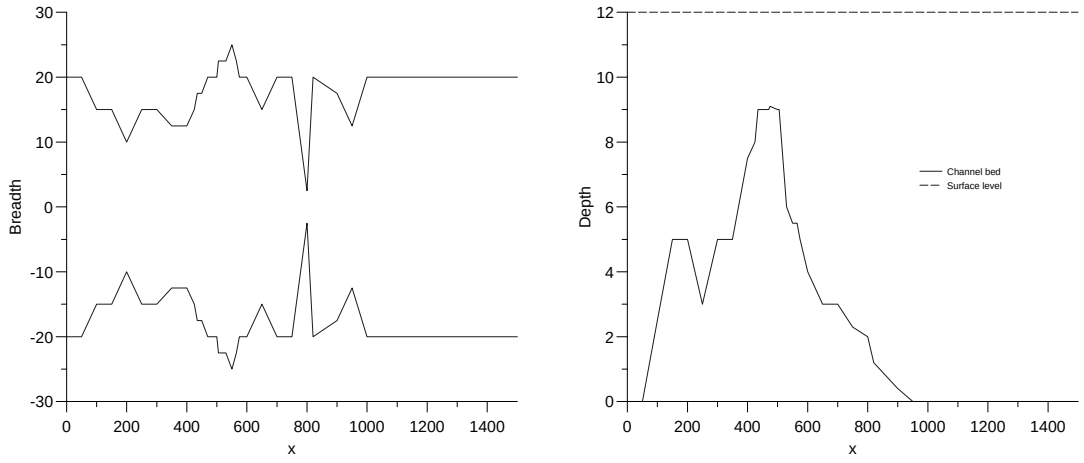

Figure 2.6: Breadth (left) and bed (right) variation for the 'tidal flow' test case.

The comparison is made between first order, slope limited and flux limited schemes combined with pointwise and upwind source term discretisations: in all high resolution cases the Minmod limiter [15] has been applied. The upwind source term discretisations always produce the correct steady state solution, exact to machine accuracy and indistinguishable from the exact solution in the graphs. This is not only true for the first order scheme (which has been achieved previously) but also for the high resolution TVD schemes using any flux or slope limiter on any grid in the presence of bed slope and breadth v

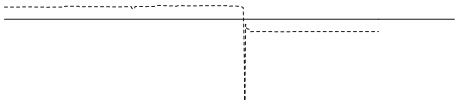

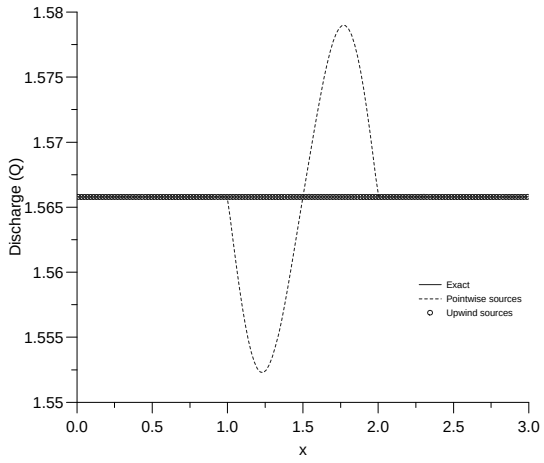
1.58
1.575
1.57
1.565
1.56
1.555
1.55
Discharge (Q)
0.0
0.5
1.0
1.5
2.0
2.5
3.0
x
Exact
Pointwise sources
Upwind sources

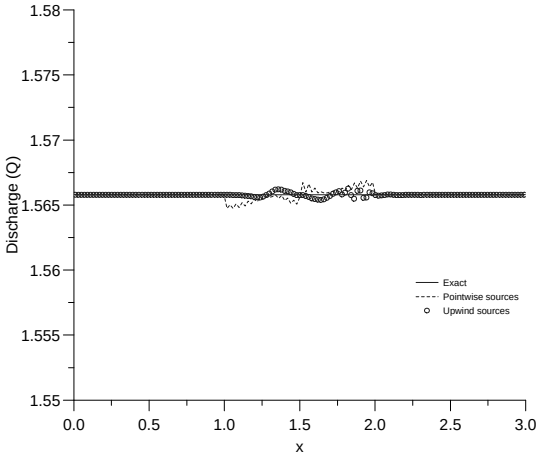
1.58
1.575
1.57
1.565
1.56
1.555
1.55
Discharge (Q)
0.0
0.5
1.0
1.5
2.0
2.5
3.0
x
Exact
Pointwise sources
Upwind sources

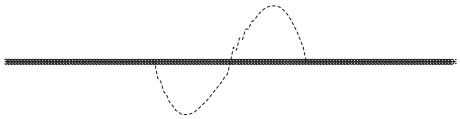

case where the latter is unable to attain a symmetric solution. The position and strength of the hydraulic jump is predicted accurately by all of the schemes, although there is a small discrepancy in the discharge at the discon

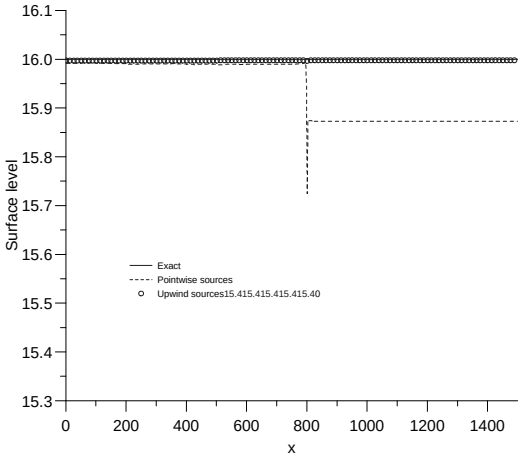
16.1
16.0
15.9
15.8
15.7
15.6
15.5
15.4
15.3
Surface level
0
200
400
600
800
1000
1200
1400
x
Exact
Pointwise sources
Upwind sources15.415.415.415.415.40

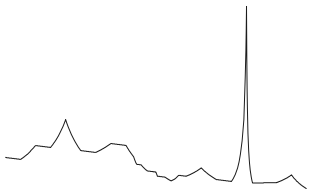

the solution to remain free of unwanted oscillations (a value of 0.1 was used in the second order case compared with 0.8 for the first order scheme). At higher CFL numbers the accuracy of the solutions is comparable to the accuracy of those obtained with the simpler source term discretisations. This is due to the fact that the TVD condition only applies in the absence of source terms. Note though that, as in the still water test, even though the pointwise source discretisation gives a reasonable approximation to the depth, it is very poor at predicting the flow velocity.

3 Higher dimensions

The following analysis is presented for the two-dimensional case but can be applied simply in three dimensions as well. The conservative form of a system of conservation laws with additional source terms is expressed as

$$\underline{U}_t + \underline{F}_x + \underline{G}_y \;=\; \underline{S}\,, \tag{3.1}$$

in which there are now two flux vectors, denoted by $\underline{F} = \underline{F}(\underline{U})$ and $\underline{G} = \underline{G}(\underline{U})$. The case where the fluxes depend on a quantity other than the flow variables is not presented here, having no obvious application to two-dimensional shallow water flows, but can be dealt with in a similar manner to the one-dimensional case presented in Section 2.2.

A combination of a standard finite volume approximation of the flux terms on an arbitrary polygonal mesh (although only triangular and quadrilateral meshes will be considered in the results) and a forward Euler discretisation of the time derivative leads to the conservative difference scheme,

$$\underline{U}_i^{n+1} \;=\; \underline{U}_i^n - \frac{\Delta t}{V_i}\sum_{l=1}^{N_e} L_{il}\,(\underline{F}^*_{il}, \underline{G}^*_{il})\cdot \hat{\vec{n}}_{il} + \frac{\Delta t}{V_i}\,\mathbf{SFcas}$$

For simplicity the scheme will again be assumed to be a cell centre discretisation in which the control volumes coincide with the mesh cells, although the techniques may also be applied to other types of scheme. The following analysis runs along similar lines to that presented in previous sections for the one-dimensional case.

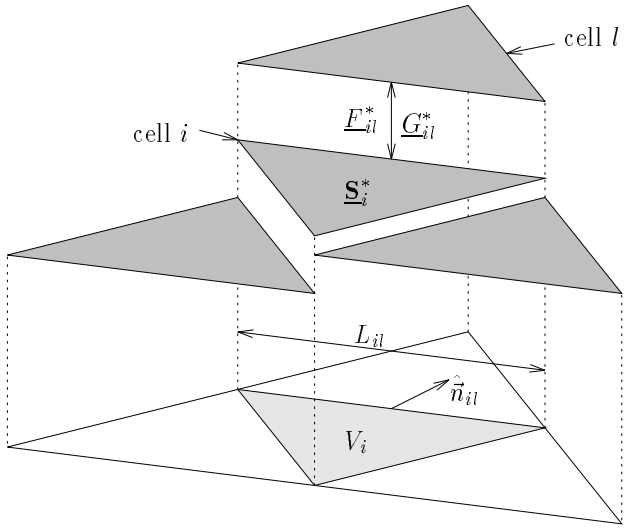

Figure 3.1: Numerical fluxes and sources for the cell centre scheme.

3.1 The first order scheme

The numerical fluxes which lead to the first order Roe's scheme in two dimensions are given by

$$(\underline{F}^*_{il}, \underline{G}^*_{il}) \cdot \hat{\vec{n}}_{il} \;=\; \frac{1}{2}(\underline{F}_i + \underline{F}_l, \underline{G}_i + \underline{G}_l) \cdot \hat{\vec{n}}_{il} - \frac{1}{2}\left(\tilde{\mathbf{R}}|\tilde{\mathbf{\Lambda}}|\tilde{\mathbf{R}}^{-1}\Delta\underline{U}\right)_{il} , \tag{3.3}$$

in which the eigenvectors and eigenvalues which are needed to construct $\tilde{\mathbf{R}}$ and $\tilde{\mathbf{\Lambda}}$ are now those of the matrix $\tilde{\mathbf{C}}_n = (\tilde{\mathbf{A}}, \tilde{\mathbf{B}}) \cdot \hat{\vec{n}}$, where

$$\tilde{\mathbf{A}} \approx \frac{\partial \underline{F}}{\partial \underline{U}} \quad \text{and} \quad \tilde{\mathbf{B}} \approx \frac{\partial \underline{G}}{\partial \underline{U}} \tag{3.4}$$

are the linearised flux Jacobians. It can be seen that the numerical flux is similar in form to that used in one dimension (2.6). In particular, $\tilde{\cdot}$ again denotes the evaluation of a quantity at its Roe-average state.

Since the two-dimensional scheme is based on Riemann solvers oriented perpendicular to the edges of the grid cells the decomposition also bears a strong resem

denoted $\tilde{\cdot}$ are evaluated at the appropriate Roe-average state [11] then the flux differences can be written in the decomposed form

$$\Delta(\underline{F},\underline{G})\cdot\hat{\vec{n}} \;=\; \tilde{\mathbf{C}}_n\Delta\underline{U} \;=\; \tilde{\mathbf{R}}\tilde{\mathbf{\Lambda}}\tilde{\mathbf{R}}^{-1}\Delta\underline{U} \;=\; \sum_{k=1}^{N_w}\tilde{\alpha}_k\tilde{\lambda}_k\underline{\tilde{r}}_k \tag{3.5}$$

from which it follows in much the same way as in one dimension that the scheme (3.2) is equivalent to

$$\underline{U}_i^{n+1} \;=\; \underline{U}_i^n - \frac{\Delta t}{V_i}\sum_{l=1}^{N_e} L_{il}\left(\tilde{\mathbf{R}}\tilde{\mathbf{\Lambda}}^{-}\tilde{\mathbf{R}}^{-1}\Delta\underline{U}\right)_{il} + \frac{\Delta t}{V_i}\underline{\mathbf{S}}_i^{*}\,, \tag{3.6}$$

where the superscript $\cdot^{-}$ now indicates the incoming characteristics at the appropriate edge of the control volume (see Figure 3.2). It is easily seen that this reduces to (2.7) when restricted to one dimension.

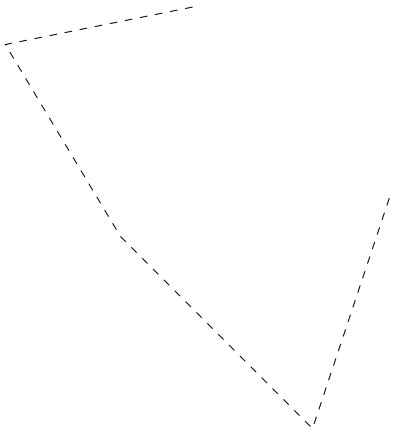

in which $V_\diamond$ is the area of the edge-cell. Now, given that the solution has already been assumed to be constant in each part of the edge-cell for the purposes of the Riemann solver, and hence the flux evaluation, the approximation reduces to

$$\tilde{\underline{\mathbf{S}}}_{il} \;=\; \left(V_\diamond \tilde{\underline{S}^0} + \sum_j \tilde{\underline{S}^1_j}\; \Delta(S^x_j, S^y_j) \cdot \vec{n} \right)_{il} , \tag{3.9}$$

where $\vec{n}$ is the normal to the edge, scaled by its length, see also (3.31). The terms within the sum may again be required to balance the flux difference, so the same Roe linearisation is used in their evaluation, and it follows that

$$\underline{F}_x + \underline{G}_y - \underline{S} \;\equiv\; \underline{0} \quad \Rightarrow \quad \left(\Delta(\underline{F}, \underline{G}) \cdot \vec{n} - \tilde{\underline{\mathbf{S}}} \right)_{il} \;=\; \underline{0} \tag{3.10}$$

throughout the domain: $\diamond_{il}$ is the edge-cell corresponding to the edge between cells i and l, as shown in Figure 3.2. The three-dimensional case is similar, with all the approximations being carried out over a face-cell with the solution being assumed constant on either side.

The two-dimensional source term can now be written as a characteristic decomposition similar to that of the flux difference (3.5), *i.e.* its linearisation can take the form

$$\tilde{\underline{\mathbf{S}}}_{il} \;=\; \left(\tilde{\mathbf{R}}\, \tilde{\mathbf{R}}^{-1} \tilde{\underline{\mathbf{S}}} \right)_{il} \;=\; L_{il} \left(\sum_{k=1}^{N_w} \tilde{\beta}_k \tilde{\underline{r}}_k \right)_{il} . \tag{3.11}$$

Evaluating this at the same Roe-average state as the flux difference means that the correct balance is attained because, at equilibrium, the decompositions give $L\mathbf{\Lambda}\mathbf{R}^{-1}\,\Delta\underline{U} = \mathbf{R}^{-1}\underline{\mathbf{S}}$. $\underline{\mathbf{S}}^*_i$ will be constructed out of contributions from each edge of the cell, with consistency assured as long as the whole of each edge-cell integral (3.11) is distributed.

The decomposition has been carried out so that, when (3.6) is combined with (3.11) to give

$$\underline{U}^{n+1}_i \;=\; \underline{U}^n_i - \frac{\Delta t}{V_i} \sum_{l=1}^{N_e} \left(\tilde{\mathbf{R}} (L \tilde{\mathbf{\Lambda}}^- \tilde{\mathbf{R}}^{-1} \Delta \underline{U} - \mathbf{I}^- \tilde{\mathbf{R}}^{-1} \tilde{\underline{\mathbf{S}}}) \right)_{il} , \tag{3.12}$$

a precise balance can be achieved when one is sought between the sources and the flux gradients.

The relationship between the two forms of the finite volume scheme, (3.2) and (3.6), can now be exploited. Substituting for $\mathbf{I}^-$ in (3.12) gives

$$\underline{U}^{n+1}_i \;=\; \underline{U}^n_i - \frac{\Delta t}{2V_i} \sum_{l=1}^{N_e} \left(\tilde{\mathbf{R}} (L \tilde{\mathbf{\Lambda}} \tilde{\mathbf{R}}^{-1} \Delta \underline{U} - \tilde{\mathbf{R}}^{-1} \tilde{\underline{\mathbf{S}}}) \right)_{il}$$

$$-\frac{\Delta t}{2V_i}\sum_{l=1}^{N_e}\left(\tilde{\mathbf{R}}(L|\tilde{\mathbf{\Lambda}}|\tilde{\mathbf{R}}^{-1}\Delta\underline{U}-\mathrm{sgn}(\mathbf{I})\tilde{\mathbf{R}}^{-1}\underline{\tilde{\mathbf{S}}})\right)_{il}\ . \quad (3.13)$$

In addition, it is easily shown that

$$\sum_{l=1}^{N_e}\Delta(\underline{F}_{il},\underline{G}_{il})\cdot$$

in which the subscripts $\cdot_{Il}$ and $\cdot_{iL}$ represent ev

3.3

and the wave strengths,

$$\begin{aligned}
\tilde{\alpha}_1 &= \frac{\Delta d}{2} + \frac{1}{2\tilde{c}}\left(\Delta(du)n^x + \Delta(dv)n^y - (\tilde{u}n^x + \tilde{v}n^y)\Delta d\right) \\
\tilde{\alpha}_2 &= \frac{1}{\tilde{c}}\left((\Delta(dv) - \tilde{v}\Delta d)\, n^x - (\Delta(du) - \tilde{u}\Delta d)\, n^y\right) \\
\tilde{\alpha}_3 &= \frac{\Delta d}{2} - \frac{1}{2\tilde{c}}\left(\Delta(du)n^x + \Delta(dv)n^y - (\tilde{u}n^x + \tilde{v}n^y)\Delta d\right) \ , \qquad (3.29)
\end{aligned}$$

complete the decomposition (3.5).

In this case, in order to provide the desired balance, the source term is written in the form (3.7), giving

$$\underline{S} = \begin{pmatrix} 0 \\ gd \\ 0 \end{pmatrix} \vec{\nabla} \cdot (h, 0) + \begin{pmatrix} 0 \\ 0 \\ gd \end{pmatrix} \vec{\nabla} \cdot (0, h)\,. \qquad (3.30)$$

At first glance this seems counterproductive, but it immediately allows the source term integral over an edge-cell to be approximated in a manner which will allow the discrete balance with the flux integral, *i.e.* it can be approximated in the form (3.9) via (3.8). This leads to

$$\tilde{\underline{\mathbf{S}}}_{il} = L_{il} \begin{pmatrix} 0 \\ g\tilde{d}\Delta h n^x \\ g\tilde{d}\Delta h n^y \end{pmatrix} , \qquad (3.31)$$

which is used to obtain the coefficients which are used in the characteristic decomposition (3.11). In this case these are

$$\tilde{\beta}_1 = \frac{1}{2}\tilde{c}\Delta h \ , \quad \tilde{\beta}_2 = 0 \ , \quad \tilde{\beta}_3 = -\frac{1}{2}\tilde{c}\Delta h\,. \qquad (3.32)$$

By construction, it follows that $\tilde{\alpha}_k\tilde{\lambda}_k - \tilde{\beta}_k = 0$ for each k, *i.e.*

$$\check{\mathbf{R}}\left(L\tilde{\mathbf{\Lambda}}\check{\mathbf{R}}^{-1}\,\Delta\underline{U} - \check{\mathbf{R}}^{-1}\tilde{\underline{\mathbf{S}}}\right) = \underline{0}\,, \qquad (3.33)$$

when the flow is quiescent, and the numerical balance is assured.

3.4 Numerical results

The test cases presented in this section are essentially a subset of those described in Section 2.3.1 for the one-dimensional schemes, but applied to the

two-dimensional shallow water equations. For the purposes of presentation, comparisons will be made between breadth-averaged solutions for channel flows and exact solutions to the corresponding one-dimensional problem. These will obviously differ slightly in the non-quiescent cases due to the simplifications inherent in the one-dimensional model but still provide an accurate guide wpro

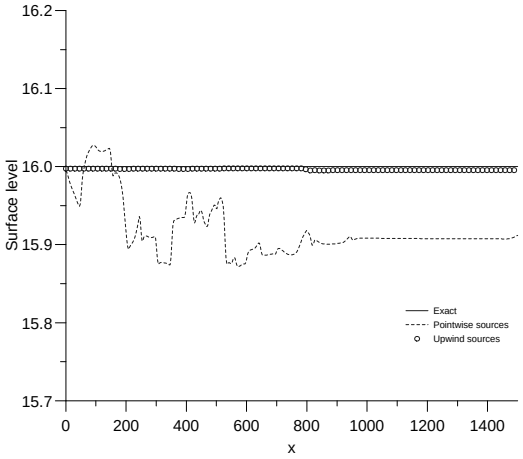
16.2
16.1
16.0
15.9
15.8
15.7
Surface level
0
200
400
600
800
1000
1200
1400
x
Exact
Pointwise sources
Upwind sources

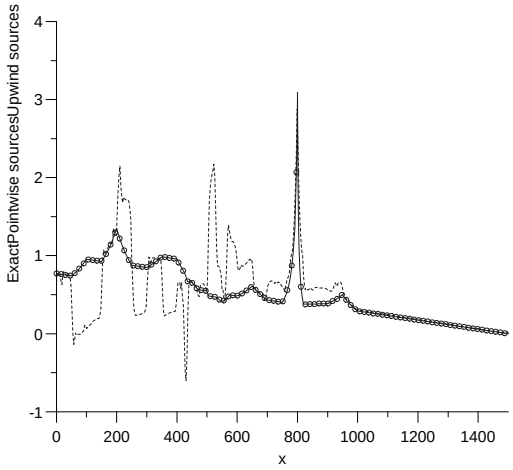
4
3
2
1
0
-1
Exact
Pointwise sources
Upwind sources
0
200
400
600
800
1000
1200
1400
x

discretisation maintains still, flat water indefinitely to machine accuracy in both the first order and the high resolution cases, see Figure 3.4. This is true of all of the channel shapes which were tested and each of the schemes described earlier in the text. The pointwise evaluation of the source term is clearly unable to match this.

Results for the tidal flow test case described in Section 2.3.1 are shown in Figure 3.5 for the same triangular grid. Again, the advantage of using the upwind source term discretisation is clearly visible and here, unlike in one dimension, the CFL number used to obtain the results is still 0.8. When the source terms are upwinded the results from the high resolution scheme are almost oscillation-free (although it must be remembered that the averaging across the channel breadth does produce a small amount of smoothing). Generally, it has been seen that the properties exhibited by the schemes in one dimension are carried over into higher dimensions.

4 Conclusions

In this paper a new method has been presented for the discretisation of source terms when they appear as part of a nonlinear system of conservation laws. Specifically, the correct approximation to the source terms is sought, given that a particular finite volume scheme has been used for the discretisation of the flux terms. Roe's scheme has been chosen here as the underlying numerical scheme, but the philosoph

source terms which provide some sort of balance with the flux derivatives. Even so, the same techniques can easily be applied to other source terms (such as those which model bed friction in the shallow water equations) which do not exhibit a precise balance, but the advantages over the simple pointwise discretisation are less obvious.

The effectiveness of these techniques has been illustrated using the one- and two-dimensional shallow water equations (the extension to three-dimensional systems of equations is straightforward, though not described here in detail), in which source terms are used to model variations in the bed topography and (in one dimension) channel breadth. Particular attention has been paid to the special case of still water, and the schemes have been constructed so that they maintain this state. In fact, the improved accuracy of the new 'upwind' discretisation of the source terms is also shown in the approximation of other steady state solutions, particularly in one dimension when flux limiters have been used, and to a great extent by time-dependent test cases as well. The improvement is less marked for slope limited schemes, indicating that a more sophisticated approximation to the source term may be necessary away from the still water steady state. This has been shown by comparison with a selection of test cases for which exact solutions are available. The advantages over the commonly-used pointwise discretisations are particularly apparent when quantities depending on the flow velocity are compared. At this stage of the research, the main problem with the new technique (a problem which also applies to the old methods) is in the modelling of time-dependent problems. Here, in order to avoid spurious oscillations in the high resolution results a low CFL number has to be imposed (0.1 in the cases tested here), and in some cases the unphysical oscillations cannot be removed completely. This is because the TVD condition which is satisfied by the scheme is only valid for the homogeneous equations. The possible construction of a TVD condition in the presence of source terms is a topic for future research. In the meantime it may prove beneficial to apply a Flux-Corrected Transport approach since it is clear from the techniques presented in this paper how the source terms should be treated for both upwind and Lax-Wendroff schemes, and the first order upwind scheme appears to be robust enough to eradicate the unwanted oscillations.

[5] P.Glaister, 'Difference schemes for the shallow water equations', Numerical Analysis Report 9/87, Department of Mathematics, University of Reading, 1987.

[6] P.Glaister, 'Prediction of supercritical flo

[16] M.E.Vázquez-Cendón, 'Improved treatment of source terms in upwind schemes for the shallow water equations in channels with irregular geometry', *J. Comput. Phys.*, **148(2)**:497–526, 1999.

[17] B.van Leer, 'Towards the ultimate conservative difference scheme V. A second order sequel to Godunov's method', *J. Comput. Phys.*, **32**:101–136, 1979.